

Study on effects of cross sectional tubes on thermal performance of concrete solar collectors: An numerical study

Maitham Jameel Zaidan^{1*} , Mohammed H. Alhamdo¹ 

¹ Mechanical Department, College of Engineering, Mustansiriyah University, Baghdad, Iraq

* Corresponding author's e-mail: mjzk1975@uomustansiriyah.edu.iq

ABSTRACT

The concepts of renewable energy utilization, encouraging sustainability, and the scientific principles of environmental conservation have become among the most critical goals that researchers are currently focusing on. Concrete and asphalt solar collectors are considered important types of solar energy collectors because they offer both economic and structural advantages. This study aims to conduct a numerical simulation using COMSOL Multiphasic software to compare the thermal performance of three non-circular tubes cross-sections extending through the solar collectors and to compare them with the commonly used circular cross-section. The cross-sections tested include semicircular, elliptical, and trapezoidal, in addition to the circular shape with a constant hydraulic diameter of 21 mm and tested sections with slab dimensions (0.5 m length, 0.16 m width, 0.05 m thickness). The same boundary conditions were applied to all cases, with a heat flux applied from the top surface and insulated the other surfaces of the slab. The results showed that the semicircular and trapezoidal cross-sections were the most efficient in transferring heat to the working fluid. This study is unique in the choice of cross-sections and contributes to scientific research by introducing innovative and unconventional methods that can enhance the efficiency of thermal and save energy systems.

Keywords: concrete solar collector, COMSOL multiphasic, simulation cross sectional tube.

INTRODUCTION

The International Energy Agency IEA's roadmap to net-zero emissions by 2050 outlines global action to limit temperature rise to 1.5 °C, confirming rapid growth in solar energy (IEA International Energy Agency, 2023). The solar collectors is one of the important thermal systems that reduce the phenomenon of harmful gas emissions and prevent riding temperatures. In addition, it contributes to providing clean energy (Lemos et al., 2014). A pavement solar collector PSC is a system that convert solar energy harvesting directly into pavement surfaces such as roads, walls of buildings, or sidewalks in to useful energy (Gholikhani et al., 2020). PSC uses asphalt or concrete that been modified to absorb more solar energy (Li et al., 2021). The absorbed heat is used for various applications such as heating buildings (Chaurasia, 2000), melting snow (Jiao et al., 2023) on the roads,

and generating electricity (Tahami et al., 2019). The main idea is use the large exposed areas to the sun into useful energy. This technology helps in energy generation and also adds value to otherwise passive infrastructure. The pavement solar collector systems have three main advantages (O'Hegarty et al., 2016): (a) It can be used as an energy source from solar radiation, since it is considered a great source of collecting solar energy at low costs. (b) Some of the stored heat can be used to heat the road during the winter to melt snow and ice (c) Access to heat during the summer helps reduce stress intensity and thus rutting (Sun, 2016). In addition to reducing the effect of heat island in large cities (Nasir et al., 2017). A pavement solar collector have three main components; the absorber part , the pipe network, and the heat transfer fluid (Dezfooli et al., 2017). The absorber part made of materials like concrete or asphalt to capture solar energy and converts it into heat (Farzan and Zaim,

2021). The second part is contain a network of embedded pipes circulates the heat transfer fluid, usually water that absorbs the heat from the pavement and transports the collected heat to a storage system or heat exchanger for practical use, forming an efficient system for harvesting solar energy (Granqvist, 2004). The heat transfer mechanism in any PSC can be represented as shown in Figure 1. Heat transfer mechanism in pavement solar collector

Most studies and research concern solar collectors used in sectional tube rings, which are commonly used for excellent operation transmission. (Abbaa and Alhamdo, 2021) (Dezfooli et al., 2017; Gholikhani et al., 2020) etc. While, few studies and research address the use of tubes with non-circular cross-sections due to their nonavailability, the ease of using circular tubes in solar energy collectors, and their efficiency in transferring heat and working fluid. Keste and Patil (2012) produced a review paper for the using of concrete as a material for solar collectors, including the potential use of metal fiber reinforced concrete. Nanhe and Gorle (2016) investigated a semicircular sectional tube in flat plate solar collector to increase the contact area between the fluid and absorber part in trapezoidal box, so they proved that this way was improved the thermal performance of flat plate solar collector. Teleszewski (2017) investigated laminar flow in a flat plate solar collector with non-circular ducts (elliptical, regular polygonal, and Cassini oval shape), focusing on forced convection. The energy equation is solved using the Boundary Element Method, and Poiseuille and Nusselt numbers are obtained for different geometrical factors.

The findings indicate that a Cassini oval with $\sigma = 0.945$ is the best option for the non-circular geometries under consideration.

Rostami et al. (2020) examined the forced convection of a multiwalled carbon nanotube-water nanofluid in a flat plate solar collector using elliptical pipes instead of circular ones. they found that elliptical pipes improved exergy efficiency, output temperature, and fluid duration inside the FPSC. The maximum exergy efficiency was 7.1%, while the maximum value was 0.10% for $v = 0.10\%$ and when parameters were changed, the variation in energy efficiency decreased. Muhsin and Alhamdo (2020) investigated that the rectangular tube sections was the most effective type, with a 36% increase in thermal efficiency when compared to circular tubes and increase 39.39% with adding fins to the rectangular cross section. Jebasingh et al. (2022) replaced the circular tube with an elliptical tube to study its performances after absorb the heat to the working fluid with three flow rates (0.028, 0.021 and 0.014 kg/s) in Tamil Nadu South of India. Islam et al. (2023) investigated numerically that using a square tube riser in FPC improves the rate of useful heat transfer of the collector and enhancing thermal efficiency compared to the use of circular and rectangular riser tubes reached to 8.1% under the same operating conditions. Since, The average efficiency with the circular tube is 65.95%, while the square tube 70.44%. The aim of the research paper is to investigate theoretically and experimentally thermal performance of pavement solar collectors PSCs and optimized pipe cross sectional shape for heat storage and extract in roofs and walls buildings.

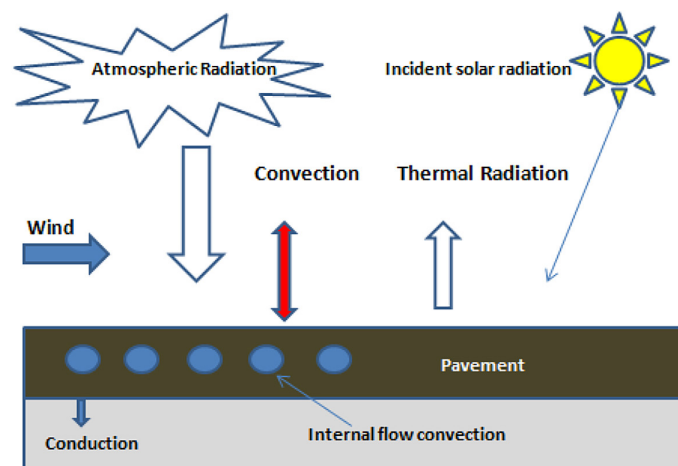


Figure 1. Heat transfer mechanism in pavement solar collector

SIMULATION PROCEDURE

Initially, SolidWorks software was used to design the solar collector, split the materials and saved the geometry file in a suitable extension for simulation in COMSOL Multiphysics software. In the COMSOL software the appropriate physical model was chosen, then the previously prepared geometry was imported. Boundary conditions established in this investigation were set,. In order to achieve the acceptable results, the FEM mesh and grids was made with the suitable shapes and sizes. The simulation has been done, and once it was finished running, then post-processing and data visualization were viewed as shown in Figure 2.

Model depiction

For the computational analysis, a simplified 3D model of the pavement solar collector was adopted, split it into three domains: the solid material of pavement domain, the fluid domain inside the tubes, and the tubes material domain. This model was simulated the heat transfer within the collector, providing the thermal performance under the boundary conditions. The dimensions of the pavement solar collector, including the thickness of the pavement layer, the diameter and material of the tubes, and the mass flow rate of the working fluid. Four different cross sectional shapes of copper tube were tested: circular,

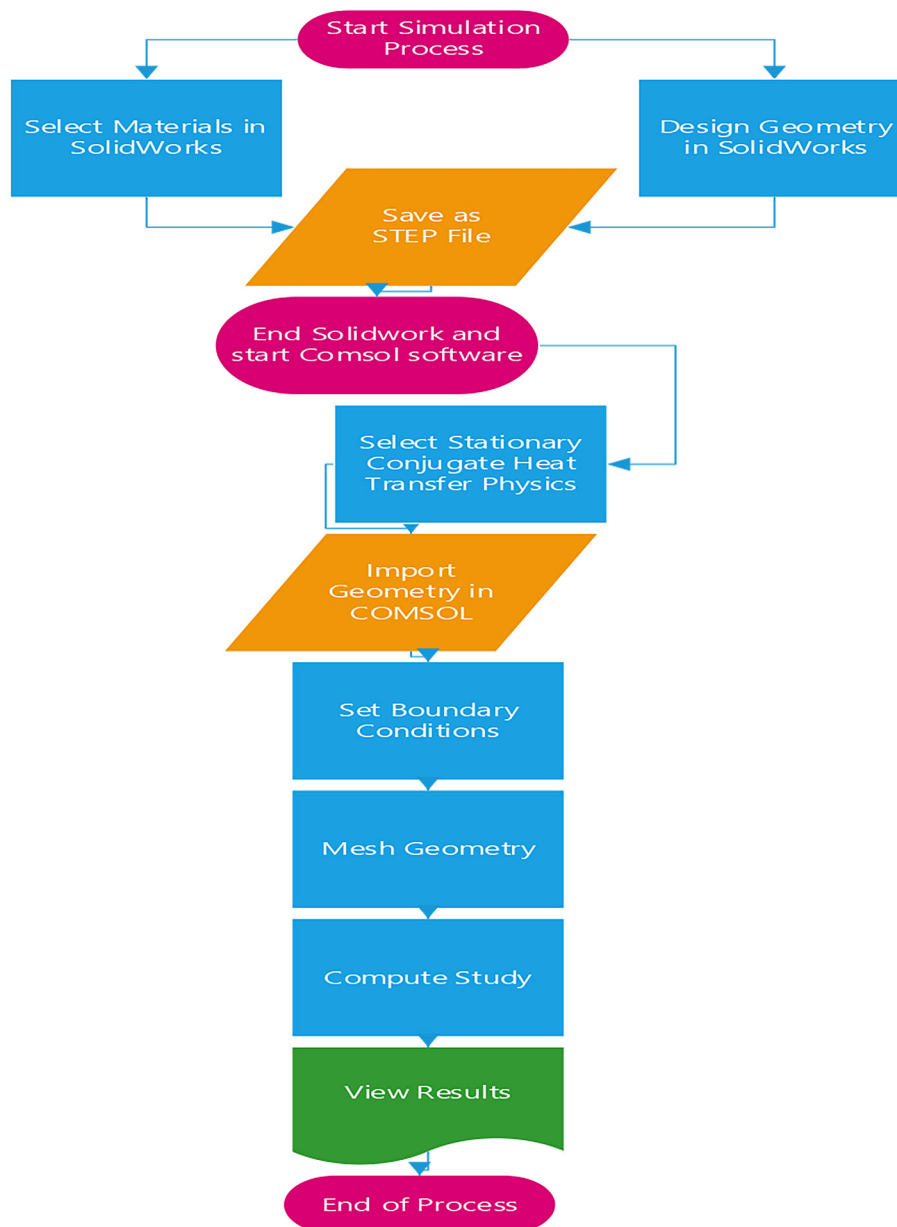


Figure 2. Simulation process flowchart

elliptical, semi-circular, and trapezoidal that the same hydraulic diameter 21 mm, as shown in Figure 3, with slab dimensions (0.5 m length, 0.16 m width, 0.05 m thickness) and boundary conditions values for all sections to evaluate which one the optimum in thermal performance as shown in Table 1.

Assumptions

- The pavement material in the PSC is homogeneous that means its thermal and physical properties are constant during simulation.
- Steady state heat transfer because of constant boundary conditions, also the reading of temperatures has been captured after the system reached the thermal equilibrium.
- No convection heat transfer between the ambient and upper surface of PSC
- The heat resistance between adjacent layers in the PSC was assumed little for their near contact.
- The fluid in the tubes inside PSC was incompressible and laminar flow.
- Newtonian – one phase fluid.

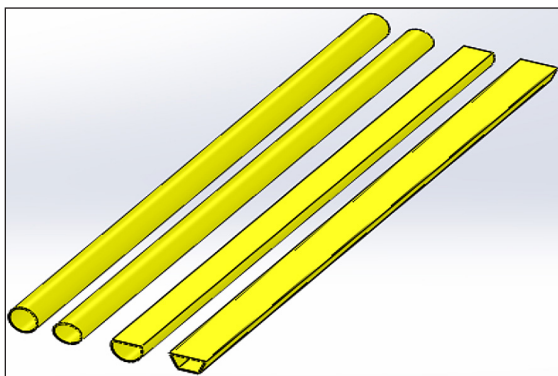


Figure 3. Tubes cross sectional shape

The governing equations

- The continuity equation

$$\nabla \cdot (\mathbf{v}) = 0 \tag{1}$$

- The momentum equation

$$\frac{\partial(\rho\mathbf{v})}{\partial t} + \nabla \cdot (\rho\mathbf{v}\mathbf{v}) = -\nabla p + \nabla \cdot \boldsymbol{\tau} + \rho\mathbf{g} + \mathbf{F} \tag{2}$$

- The energy equation

$$\frac{\partial(\rho E)}{\partial t} + \nabla \cdot (\rho\mathbf{v}(E + p)) = \nabla \cdot \left(k_{\text{eff}}\nabla T - \sum_j h_j \cdot \mathbf{J}_j + \boldsymbol{\tau}_{\text{eff}} \cdot \mathbf{v} \right) + S_h \tag{3}$$

where: ∇p represent pressure forces; $\nabla \cdot \boldsymbol{\tau}$ represent viscous forces; $\rho\mathbf{g}$ is the effect of gravity on fluid flow; the term \mathbf{F} represents any external forces act on the fluid (Bergman et al., 2011).

Boundary conditions

In numerical simulation boundary conditions were established for the test sections to obtain perfect results and compare these results for different cases. The upper surface of PSC was only exposed surface to heat flux from the lumps with a value of 600 w/m², but the other surfaces were considered fully insulated. It was assumed that the fluid inlet velocity was 0.01 m/s with a temperature of 293 K. The exit zone was considered an area with Zero gauge value as shown in Figure 4.

Mesh methodology

The mesh setup, including tetrahedra, prisms, triangles, quads, edge, and vertex elements, was

Table 1. Summary of modeling

Model no.	Slab dimensions	Hydraulic diameter	B.C	Tube cross section	Slab section
Model 1	0.5-0.16-0.05 m	21 mm	Heat flux: 600 W/m ² Inlet fluid: v = 0.01 m/s T = 295 k Outlet fluid: P = 0 atm	Circular	
Model 2				Elliptical	
Model 3				Semicircular	
Model 4				Trapezoidal	

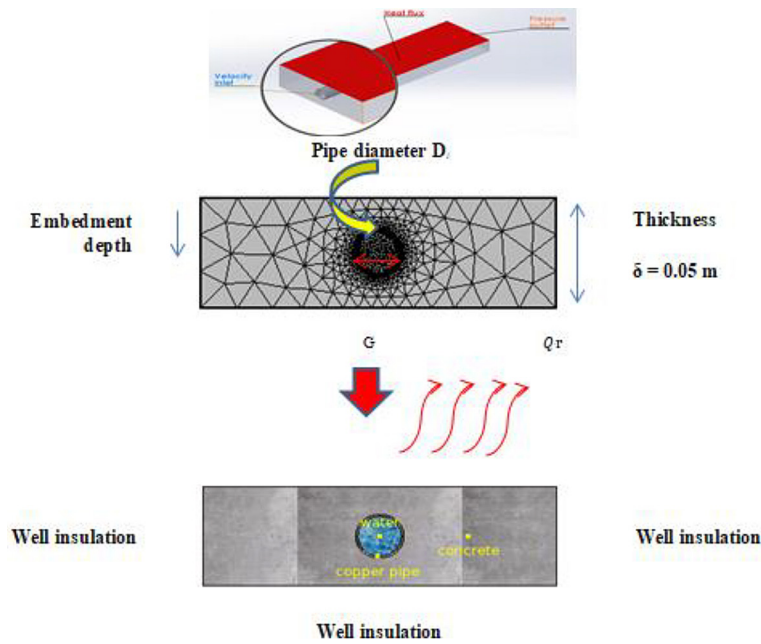


Figure 4. Dimensions and mesh of 1 test solar collector and boundary conditions

designed to divide complex geometries however matching computational accuracy. The mesh quality was maintained through element size, curvature factor, and resolution, tailored specially for fluid applications.

Mesh statistics

The Table 2 exhibits overall statistics of the mesh used in one case in this simulation study such as vertices, tetrahedral, prisms, and others, also provides key quality metrics like the minimum and average quality of elements, the ratio of element volumes, and the total volume of the mesh used.

Mesh settings and selections

The Table 3 includes maximum and minimum element sizes, curvature factors, resolutions of narrow regions, and the maximum growth rate of elements, also these are critical for optimizing the mesh to accurately capture the physics of the simulated phenomena.

Mesh independency for verification

The data in Table 4 referred the significance of mesh independence in computational simulations and it was achieved when adjustments to the mesh size no longer significantly alter the simulation outcomes, suggesting that the model

has stabilized in relation to the mesh configuration. The analysis shows that finer meshes lead to more precise predictions of thermal behavior,

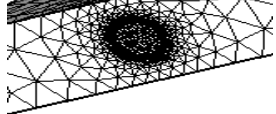
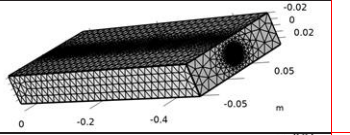
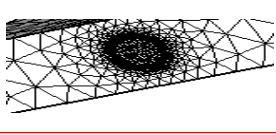
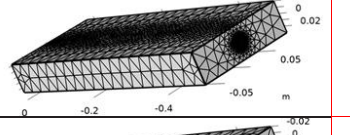
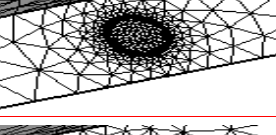
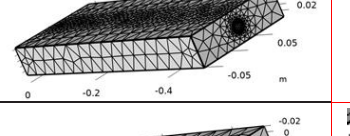
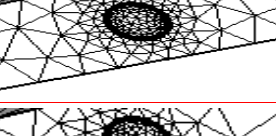
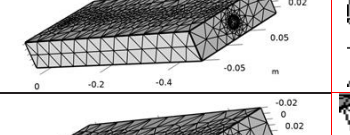
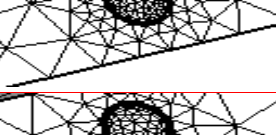
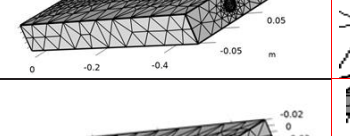
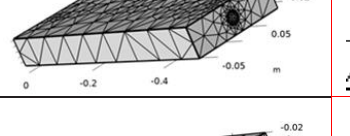
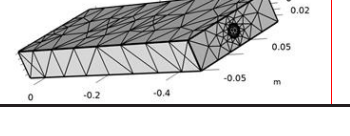
Table 2. Mesh statistics

Description	Value
Status	Complete mesh
Mesh vertices	343,320
Tetrahedra	1,721,046
Prisms	110,376
Triangles	119,528
Quads	216
Edge elements	2,126
Vertex elements	16
Total number of elements	1,831,422
Minimum element quality	0.125
Average element quality	0.6907
Element volume ratio	1.6014E-5
Mesh volume	0.003971 m ³

Table 3. Elements size

Description	Value
Maximum element size	0.0175
Minimum element size	0.00075
Curvature factor	0.3
Resolution of narrow regions	0.85
Maximum element growth rate	1.35
Predefined size	Extra fine

Table 4. Mesh independency

Predefined size	Outlet temperature (k)	Number of elements	Average element quality	Mesh used in analysis	Zoom frame
Extremely fine	325.1	2236468	0.705		
Extra fine	325.4	977403	0.7041		
Finer	326.7	219036	0.7115		
Fine	328.5	56762	0.713		
Normal	330.5	22759	0.705		
Coarse	331.4	11135	0.7134		
Coarser	332	8621	0.6783		
Extra coarse	334.3	5928	0.6338		

as indicated by the systematic reduction in outlet temperatures with increasingly finer meshes, it also reveals that as the mesh becomes finer, both the number of elements and their quality improve, approaching a state where further refinement does not substantially enhance the results but increases computational costs .

Segregated solver techniques

Achieving precision with segregated solver techniques for verification had been done in this study. The convergence of temperature in a simulation using a segregated solver to an error tolerance of less than 0.001 after number of iterations as shown in Figure 5. The segregation approach, by treating temperature as shown by

the green line-, pressure, and velocity as shown by the blue line, allowed for focused error minimization in the thermal domain. The initial conditions for temperature were chosen, reducing the computational needed to reach convergence. The mesh quality in regions of thermal activity simplify accurate temperature gradient in resolving the thermal field with high precision.

Test sections

Table 5 summarize the geometric parameters of the test sections.

Thermal properties of the test section

Table 6 summarize the thermal properties of the test section.

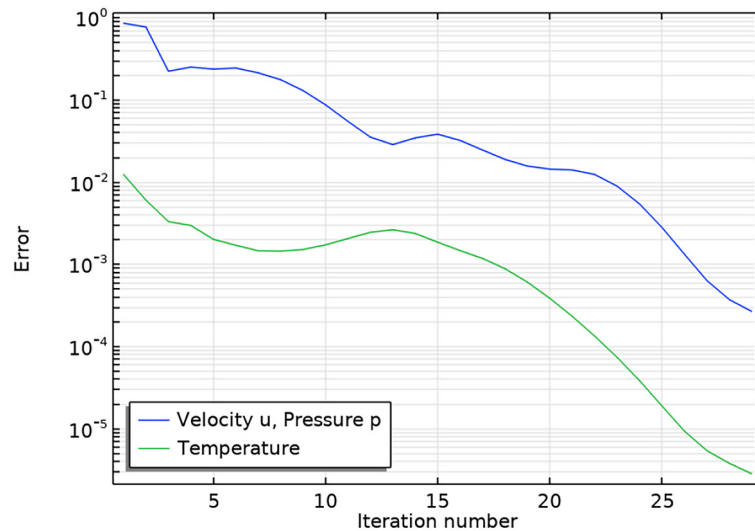


Figure 5. Thermal dynamics convergence in segregated solver

Table 5. Test section geometric parameters

Parameters	Test section
Slab width (W_s)	160 mm
Slab length (L_s)	500 mm
Slab thickness (δ_s)	50 mm
Hydraulic diameter (D_h)	21 mm
Tube cross section shape	Circular, semi-circular, elliptical, trapezoidal
Tube length (L_t)	50 mm
Tube outer diameter (D_o)	22.25 mm
Tube inner diameter (D_i)	21 mm
Tube arrangement	Straight tube
Tube material	Copper
Working fluid	Water
Pavement material	Concrete

Table 6. Thermal properties of concrete slab test section

Property	The value
Thermal conductivity	1.7 W/(m·K)
Density	2200 kg/m ³
Specific heat capacity	880 J/(kg·K)

RESULTS AND DISCUSSIONS

The simulation was implemented in finite element analysis (FEA) that achieved in COMSOL Multiphasic software, to conduct the analysis of the thermal performance of the concrete solar collector in terms of the tube cross sectional shape. The test section slab dimensions were 0.5 meters in length, 0.16 meters in width, and 0.05 meters in height, with the tube centrally placed

along the length of the slab, and the top surface of the slab exposed to a constant heat flux of 600 W/m². The remaining surfaces of the slab were thermally insulated, and water flowed inside the tube as laminar flow with low Reynolds number not exceeds 20. Four different shapes of copper tube cross-sections were tested, circular, elliptical, semi-circular, and trapezoidal those have the same hydraulic diameter value for all sections. The simulation results indicate that the semi-circular tube shape had been better in heat transfer efficiency as shown in Figure 8. This higher performance is attributed to the upper larger flat surface area of the tube exposed to the heat flux from above, enhancing the heat absorption capacity of the water flowing through the tube. After the semi-circular shape in thermal efficiency was the trapezoidal shape as shown in Figure 9, then the circular as shown in Figure 6, and finally, the elliptical shape as shown in Figure 7. The lower rate of heat transfers of the elliptical shape underscores the significance of cross sectional design in the thermal performance of PSCs. Furthermore the fluid motions within the semicircular and trapezoidal tubes were induced turbulent flow conditions at lower velocities that enhance the heat transfer to the water. This turbulence helps mixing within the fluid, reducing the creation of thermal boundary layers and ensuring a more uniform temperature distribution. In the graphical representation for the results of the comparison as shown in Figure 10, a convergence of results was observed between the semi-circular and trapezoidal shapes, while a similar closeness in outcomes was noted between the elliptical and circular

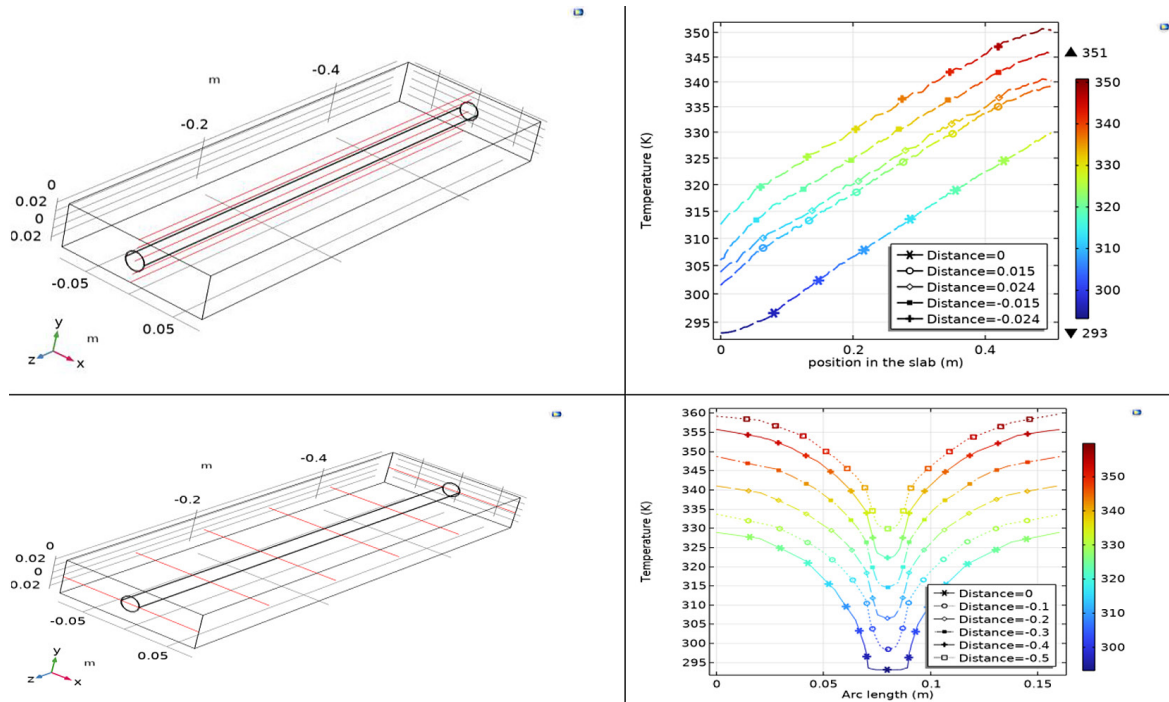


Figure 6. Temperature distribution in the cut lines through the test section with a circular tube

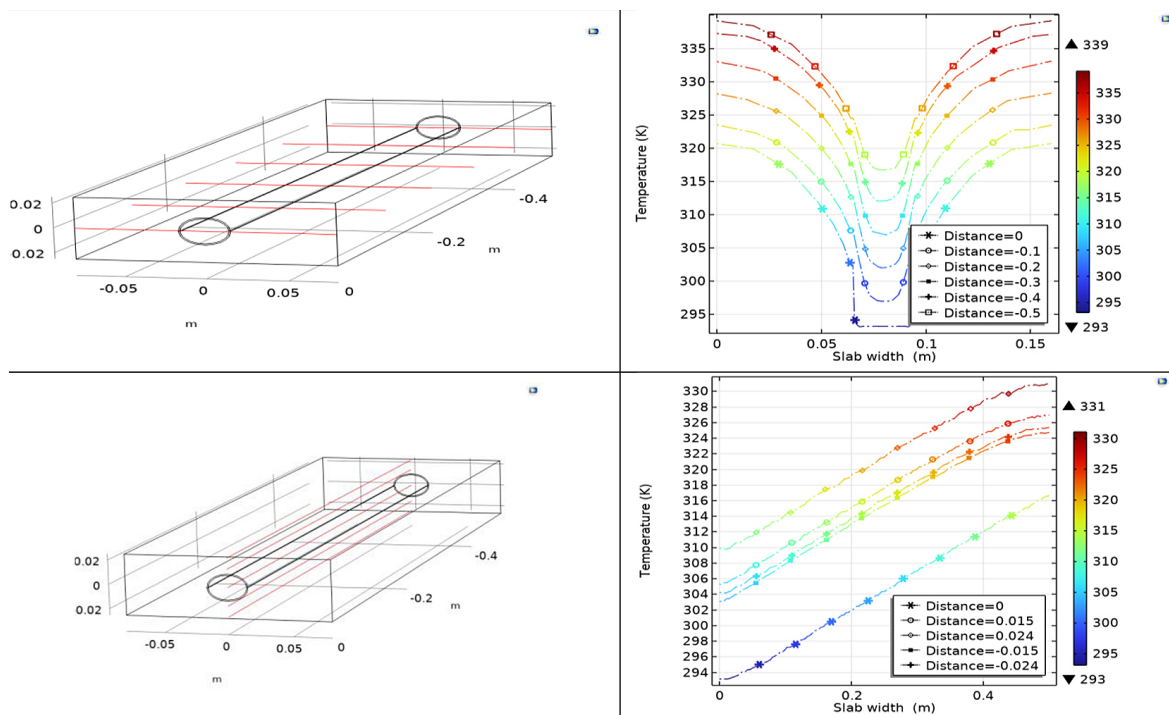


Figure 7. Temperature distribution in the cut lines through the test section with the elliptical tube

configurations. On the contrary, the elliptical and circular shapes were found to exhibit less disruption to laminar flow, leading to a less pronounced enhancement in heat transfer efficiency. The comparative analysis showed that these shapes tend to maintain a more uniform.

Local and average convection heat transfer coefficient and Nusselt number

The local heat transfer coefficient and Nusselt number assuming as internal laminar flow with constant wall heat flux in entrance region

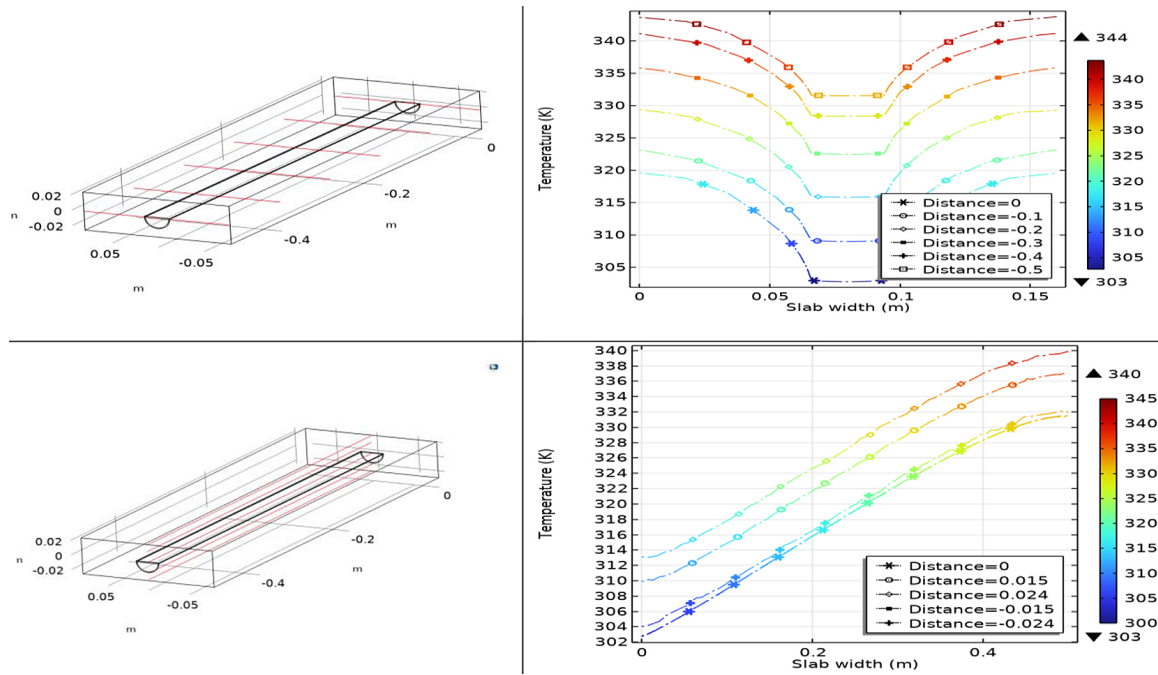


Figure 8. Temperature distribution in the cut lines through the test section with the semicircular tube

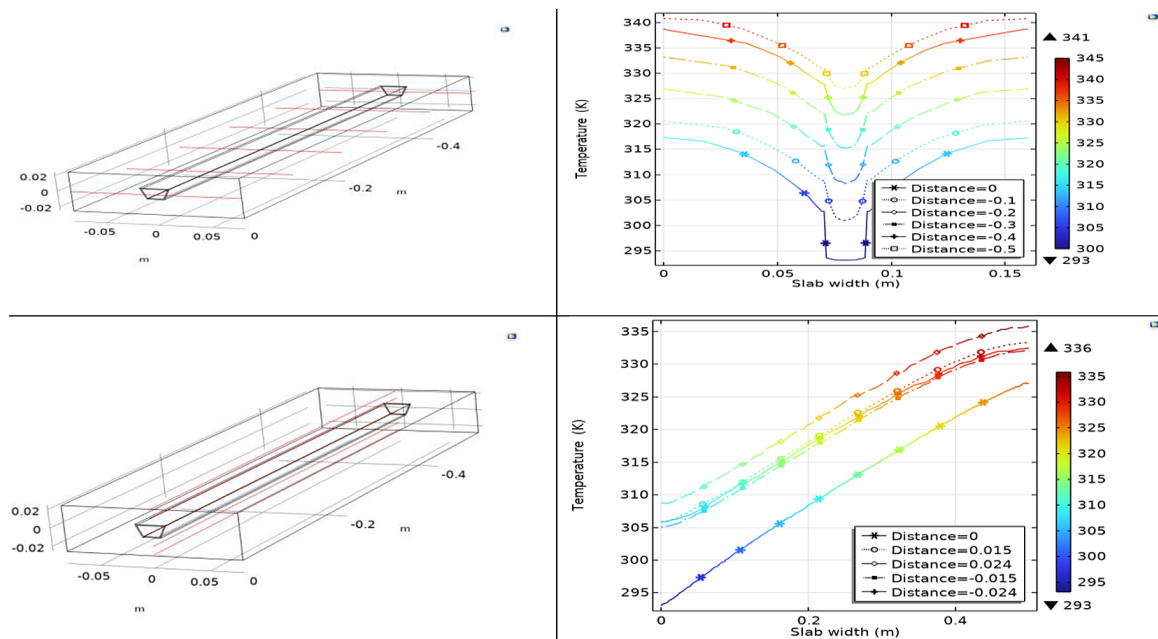


Figure 9. Temperature distribution in the cut lines through the test section with the trapezoidal tube

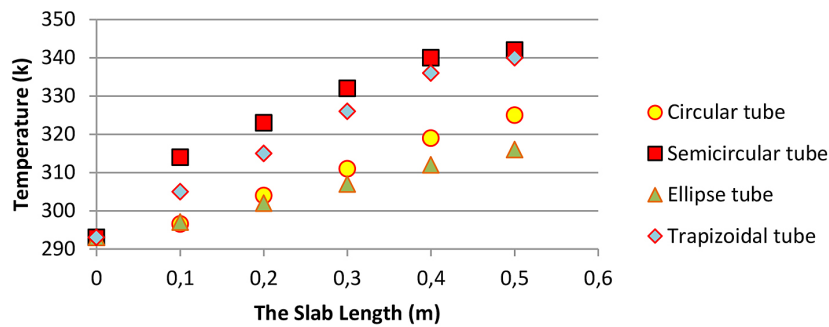


Figure 10. Comparative of tube geometries on water temperature

before the flow become fully developed and this flow called “thermal developing flow” with low Reynolds number (Jacimovic et al., 2018). They were calculated at set of points along the tube from the entrance region to the exit, as a function of the Reynolds number Re , Prandtl number Pr , and the ratio of the tube length L to the hydraulic diameter D_h . Reynolds and Prandtl numbers for each geometry were assumed constant, while the ratio of the tube length L to the hydraulic diameter D_h was varied depended on position on the tube. The results obtained by COMSOL multiphase software program simulations for trapezoidal, circular, semicircular,

and elliptical cross-sectional tubes detect varying heat transfer performance characterized by the local convection heat transfer coefficient and the local Nusselt number. The circular tube shows h_x decreasing from $652 \text{ W/m}^2\cdot\text{k}$ to $233 \text{ W/m}^2\cdot\text{k}$ and N_{ux} from 21.733 to 7.766, with averages of $401.2857 \text{ W/m}^2\cdot\text{k}$ and 13.375, respectively, as shown in Figure 11. For the semi-circular tube, h_x decreases from $659 \text{ W/m}^2\cdot\text{k}$ to $243 \text{ W/m}^2\cdot\text{k}$ and N_{ux} from 21.96 to 8.1, with averages of $412.2857 \text{ W/m}^2\cdot\text{k}$ and 13.739 as shown in Figure 12. For the trapezoidal tube geometry, decreases from $650 \text{ W/m}^2\cdot\text{k}$ to $235 \text{ W/m}^2\cdot\text{k}$, and N_{ux} decreases from 21.66 to 7.833,

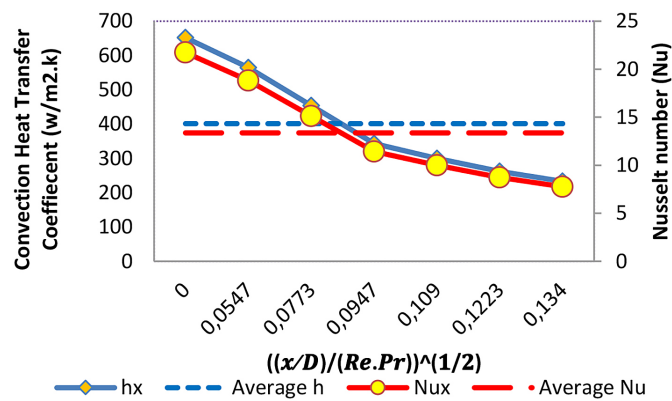


Figure 11. Heat transfer coefficient and Nusselt number for circular cross sectional tube

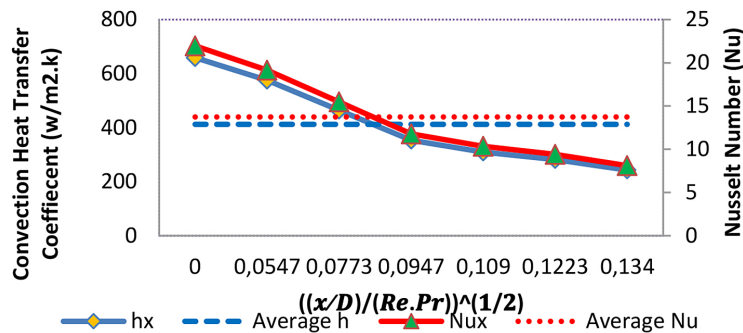


Figure 12. Heat transfer coefficient and Nusselt number for semi-circular cross sectional tube

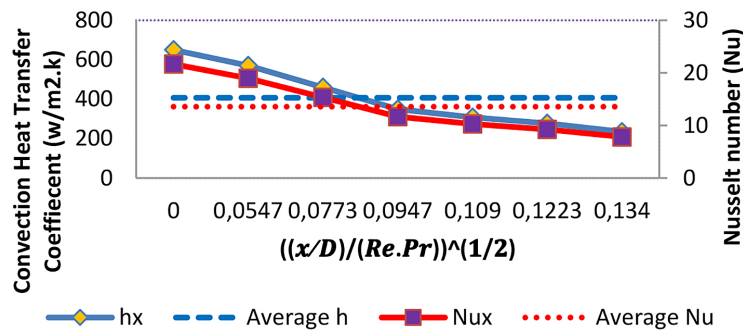


Figure 13. Heat transfer coefficient and Nusselt number for trapezoidal cross sectional tube

with an average h of $407.1429 \text{ W/m}^2\cdot\text{k}$ and an average Nu of 13.5688 as shown in Figure 13. The elliptical tube h_x decreased from $640 \text{ W/m}^2\cdot\text{k}$ to $223 \text{ W/m}^2\cdot\text{k}$ and Nu_x from 21.333 to 7.43 , with averages h of $392.4286 \text{ W/m}^2\cdot\text{k}$ and Nu 13.0755 as shown in Figure 14. The semicircular and trapezoidal tube geometry has a better performance in heat transfer characteristics than the elliptical tube, which shows lower performance. Figure 15 shows average heat transfer coefficient and Nusselt number for each tube geometry.

The temperature distribution contours

The temperature distribution contours of the four pipe cross-sections shapes had been compared to estimate the thermal performance in the test section pavement solar collectors. The semi-circular tube section had been shown the best representation of the temperature gradient, particularly highlighting the temperatures of the water exiting the pipe because of the uniformity of the heat distribution around the pipe and the flat upper surface that exposed to heat flux as shown in Figure 18. Next the semi-circular section, the trapezoidal shape that had

a similarly pattern of temperature distribution, and slightly less notable than the semi-circular case. The rate of heat transfer had remained effective, but the temperature gradients had appeared less uniform, particularly at the corners of the trapezoidal section where heat dissipation had been more uneven as shown in Figure 19. The circular section had shown less heat transfer patterns, with the temperature distribution more uniform around the pipe but not as clearly highlighting the exit temperatures of the water. The heat distribution had been more radial, with less distinction between the heated and unheated zones, resulting in a slightly lower efficiency in terms of visible temperature variation as shown in Figure 16. The elliptical section had the least temperature contours among the compared shapes as shown in Figure 17.

Model validation

For circular tube, which is the common tube type a good agreement validated against reference (Shah, 1978) as shown in Figure 20. The average percentage error about 17.1% between the obtained results and the referred reference

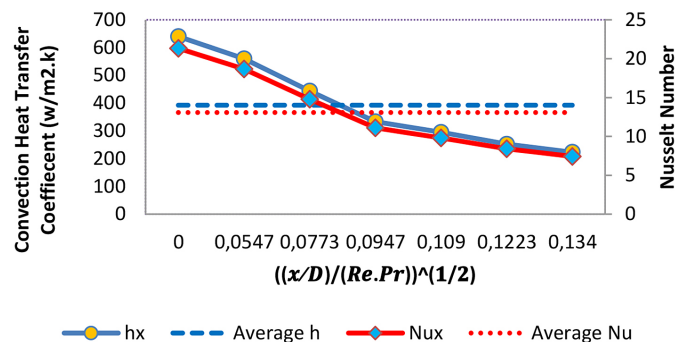


Figure 14. Heat transfer coefficient and Nusselt number for elliptical cross sectional tube

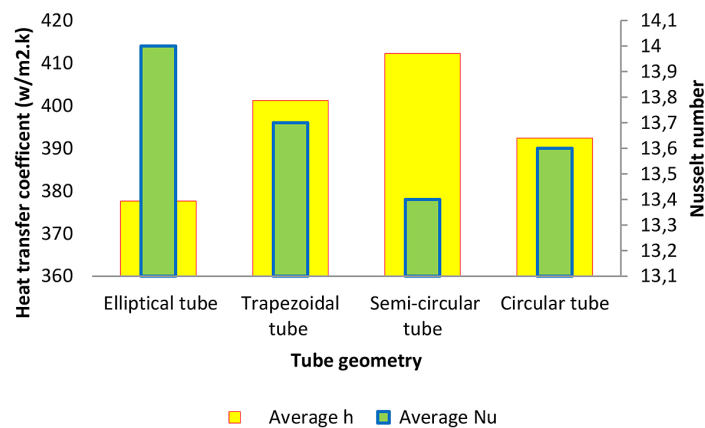


Figure 15. Average heat transfer coefficient and Nusselt number for each tube geometry

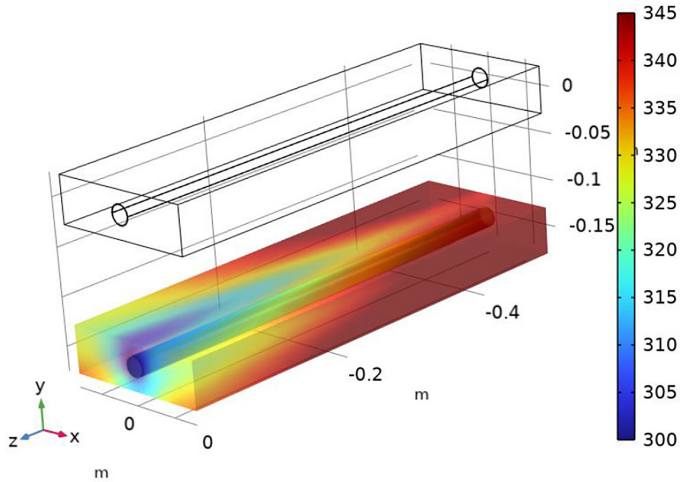


Figure 16. Circular tube contours for test section

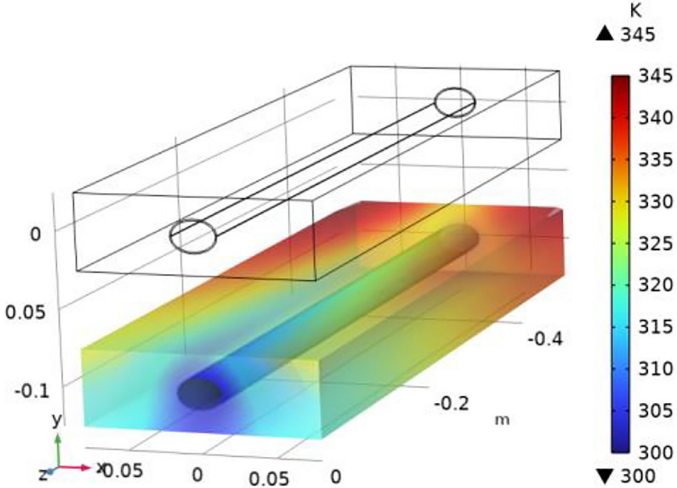


Figure 17. Elliptical tube contours for the test section

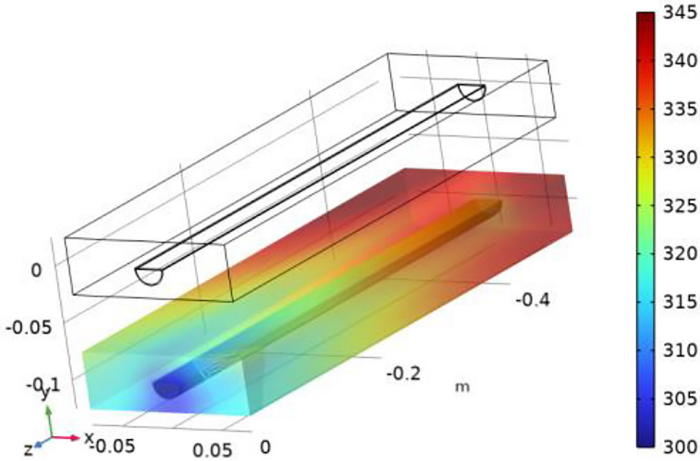


Figure 18. Semi-Circular tube contours for the test section

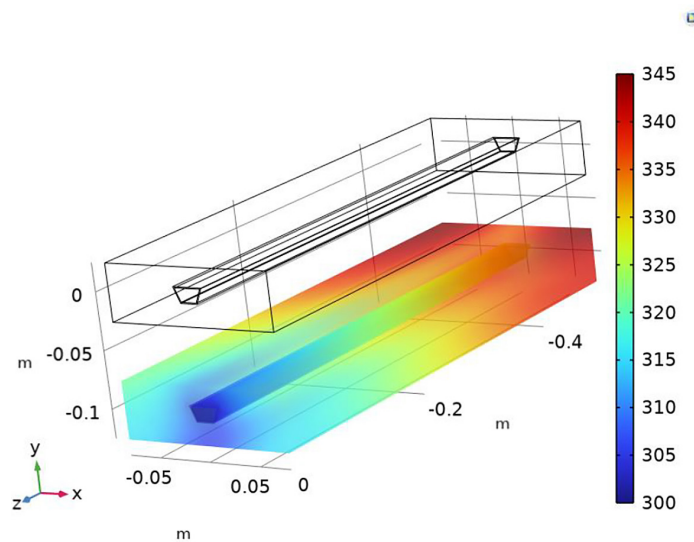


Figure 19. Trapezoidal tube contours for the test section

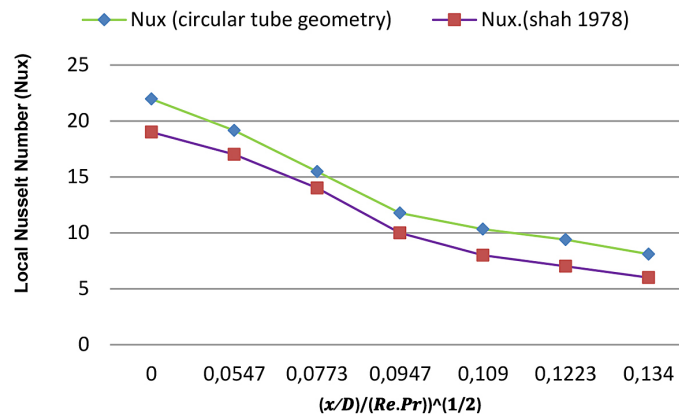


Figure 20. Nusselt number in entrance region of around duct (Shah, 1978)

CONCLUSIONS

This numerical study addressed the impact of the shape of pipe sections passing through the solar collectors on thermal performance by testing three rarely used non-circular sections in addition to the commonly used circular section. The study proved that the thermal efficiency of the solar collector with semi-circular and trapezoidal sections is better in performance than the test sample with circular and elliptical sections. The high performance of tube geometry is attributed to the upper larger flat surface area exposed to the heat flux from above, enhancing the heat absorption capacity of the water flowing through the tube. The elliptical and circular shapes were found to exhibit less disruption to laminar flow, leading to a less pronounced enhancement in heat transfer efficiency. The comparative analysis showed that these shapes tend to maintain a more uniform.

Acknowledgements

The authors would like to thank Mustansiriyah University (www.uomustansiriyah.edu.iq) Baghdad – Iraq for its support in the present work.

REFERENCES

1. Abbaa, F.A., Alhamdo, M.H. (2021). Progress in Solar Energy and Engineering Systems. *Journal Homepage: [Http://ieta.org/journals/Psees](http://ieta.org/journals/Psees)*, 5(1), 17–25.
2. Bergman, T.L., Lavine, A.S., Incropera, F.P., Dewitt, D.P. (2011). *Introduction to heat transfer*. John Wiley & Sons.
3. Chaurasia, P.B.L. (2000). Solar water heaters based on concrete collectors. *Energy*, 25(8), 703–716. [https://doi.org/10.1016/S0360-5442\(99\)00091-2](https://doi.org/10.1016/S0360-5442(99)00091-2)
4. Dezfooli, A.S., Nejad, F.M., Zakeri, H., Kazemifard,

- S. (2017). Solar pavement: A new emerging technology. *Solar Energy*, 149, 272–284. <https://doi.org/10.1016/J.SOLENER.2017.04.016>
5. Farzan, H., Zaim, E.H. (2021). Feasibility study on using asphalt pavements as heat absorbers and sensible heat storage materials in solar air heaters: An experimental study. *Journal of Energy Storage*, 44. <https://doi.org/10.1016/j.est.2021.103383>
 6. Gholikhani, M., Roshani, H., Dessouky, S., Papagiannakis, A.T. (2020). A critical review of roadway energy harvesting technologies. In *Applied Energy* (Vol. 261). <https://doi.org/10.1016/j.apenergy.2019.114388>
 7. Granqvist, C.G. (2004). Materials for Solar Energy. In C. J. Cleveland (Ed.), *Encyclopedia of Energy* (pp. 845–858). Elsevier. <https://doi.org/https://doi.org/10.1016/B0-12-176480-X/00325-9>
 8. IEA International Energy Agency. (2023). *global energy-related carbon dioxide emissions to net zero by 2050*. <https://www.iea.org/reports/net-zero-by-2050>
 9. Islam, R., Ali, M.H., Pratik, N.A., Lubaba, N., Miyara, A. (2023). Numerical analysis of a flat plate collector using different types of parallel tube geometry. *AIP Advances*, 13(10).
 10. Jacimovic, B., Genic, S., Lelea, D. (2018). Calculation of the heat transfer coefficient for laminar flow in pipes in practical engineering applications. *Heat Transfer Engineering*, 39(20), 1790–1796.
 11. Jebasingh, V.K., Divya Johns, J., Arunkumar, T. (2022). Assessment of circular and elliptical absorber tube in solar parabolic trough collector. *International Journal of Ambient Energy*, 43(1), 873–878.
 12. Jiao, W., Sha, A., Liu, Z., Jiang, W., Hu, L., Qin, W. (2023). Analytic investigations of snow melting efficiency and temperature field of thermal conductive asphalt concrete combined with electrical-thermal system. *Journal of Cleaner Production*, 399, 136622.
 13. Keste, A.A., Patil, S.R. (2012). Investigation of concrete solar collector: a review. *IOSR J. Mech. Civ. Eng*, 6, 26–29.
 14. Lemos, J. M., Neves-Silva, R., & Igreja, J. M. (2014). *Adaptive Control of Solar Energy Collector Systems*.
 15. Li, X., Wang, Y.M., Wu, Y. L., Wang, H.R., Chen, M., Sun, H.D., Fan, L. (2021). Properties and modification mechanism of asphalt with graphene as modifier. *Construction and Building Materials*, 272, 121919. <https://doi.org/10.1016/J.CONBUILDMAT.2020.121919>
 16. Muhsin, N.M.B., Alhamdo, M.H. (2020). Study experiential and numerical for investigation the efficiency inside building structure. *European Journal of Molecular & Clinical Medicine*, 7(06), 1917–1936.
 17. Nanhe, V.B., Gorle, R.D. (2016). *Performance Analysis of Flat Plate Solar Water Collector using Trapezoidal shape and Semi-circular Tubes: A Review*. 2012–2015.
 18. Nasir, D.S.N.M., Hughes, B.R., Calautit, J.K. (2017). Influence of urban form on the performance of road pavement solar collector system: Symmetrical and asymmetrical heights. *Energy Conversion and Management*, 149, 904–917. <https://doi.org/10.1016/J.ENCONMAN.2017.03.081>
 19. O’Hegarty, R., Kinnane, O., McCormack, S. (2016). Parametric analysis of concrete solar collectors. *Energy Procedia*, 91, 954–962. <https://doi.org/10.1016/j.egypro.2016.06.262>
 20. Rostami, S., Sepehrirad, M., Dezfulizadeh, A., Hussein, A.K., Shahsavvar Goldanlou, A., Shadloo, M.S. (2020). Exergy optimization of a solar collector in flat plate shape equipped with elliptical pipes filled with turbulent nanofluid flow: a study for thermal management. *Water*, 12(8), 2294.
 21. Shah, R.K. (1978). Laminar Flow Forced Convection in. *Ducts, Supp. 1 of Advances in Heat Transfer*, 153–195.
 22. Sun, L. (2016). Distribution of the temperature field in a pavement structure. *Structural Behavior of Asphalt Pavements*, 61–177. <https://doi.org/10.1016/B978-0-12-849908-5.00002-X>
 23. Tahami, S.A., Gholikhani, M., Nasouri, R., Dessouky, S., Papagiannakis, A.T. (2019). Developing a new thermoelectric approach for energy harvesting from asphalt pavements. *Applied Energy*, 238. <https://doi.org/10.1016/j.apenergy.2019.01.152>
 24. Teleszewski, T.J. (2017). A numerical investigation of laminar forced convection in a solar collector with non-circular duct. *E3S Web of Conferences*, 22, 1–8. <https://doi.org/10.1051/e3sconf/20172200177>